Functionalization and exfoliation of graphite with low temperature pulse plasma in distilled water

Adrien Letoffé, Stéphane Cuynet, Cédric Noël, Ludovic de Poucques, I. Royaud, Claire Hérold, Gérard Henrion, Marc Ponçot, Sébastien Fontana

ARTICLE

Functionalization and exfoliation of graphite with low temperature pulse plasma in distilled water

Received 00th January 20xx,
Accepted 00th January 20xx

DOI: 10.1039/x0xx00000x

Adrien Letoffé, Stéphane Cuynet, Cédric Noel, Ludovic de Poucques, Isabelle Royaud, Claire Hérold, Gérard Henrion, Marc Ponçot and Sébastien Fontana*

Graphene material exhibits extraordinary properties, but is difficult to produce. The present work describes the possibility of using a plasma process to exfoliate and functionalize graphite flakes. An impulse plasma phase is generated at a liquid surface for producing chemical species and shock waves in order to modify the reactive liquid and the graphite flakes as well. With this process, an industrial graphite was treated. A 20% thickness diminution was observed, with the formation of a random turbostratic structure. The exfoliation comes along with a small functionalization of the surface. Even after treatment, the graphite flakes present a low defect density compared with other treated graphite obtained by more conventional chemical treatments. This process is a new way to exfoliate graphite and to produce functionalized graphenic materials.

A Introduction

Carbon based materials have attracted a lot of attention in the material research field, because of the many different structures, like carbon nanotubes, fullerenes, graphite and graphene, and their respective properties. Graphene is a sp^2-hybridized one-atom thick carbon structure arranged in a hexagonal pattern. The graphene properties have led to an abundance of interest since 2004. Graphene exhibits high mechanical properties[1,2] with a mechanical strength amongst the highest observed, but also with a high thermal conductivity,[3] a high specific surface area[4] and a transparency over 97%.[5,6] The main property of graphene is its zero-overlap semi-conductor structure, displaying a very high electrical conductivity.[7] With such properties, graphene is a good candidate for numerous applications like chemical filtering,[8,9] energy storage and batteries,[10,11] flexible electronics,[5] or for the elaboration of conductive polymers.[12]

In order to produce the large quantities of graphene needed for such applications, a huge variety of elaboration methods have been developed. There are two groups of synthesis methods: the top-down ones, for which single layers of graphene are removed from a macroscopic carbon material such as graphite, as the "Scotch-tape" method proposed by Novoselov *et al,* and the bottom-up methods that use a carbon-based precursor to produce layers of graphene. [13] The top-down methods regroup the mechanical exfoliation, like sonication, the electrochemical and the oxidation-reduction treatment.[14-17] The classical bottom-up approach implies chemical vapour deposition (CVD) that involves a carbonaceous precursor such as methane to grow a graphene film on a substrate.[18-20] All these methods produce different quality of graphene, with wide variation in size, crystallinity, purity, and amount produced.

For instance, the CVD methods enable the production of high-quality graphene, but in low amount, and are not adaptable for industrial use.[18-20] On the other hand, chemical treatments based on acids mixture or electrochemical exfoliation can produce high quantity of graphene oxide. The obtained material, however, show a significant amount of defect, need post treatments to reduce them, and are more often composed of few layers graphene (between 2 and 5 layers) than pure graphene.[21] Those defects degrade the properties of graphene flakes, like the electrical conductivity.[17] Methods able to produce large quantity of graphene without defect are still a challenge.

In the last decades, a new type of treatments using plasma-liquid interaction has been developed to synthesize nanoparticles. Plasma treatments have been used in numerous studies, and have focused on glow discharge electrolysis or on the breakdown of dielectric liquid. Plasma discharges are now used in a variety of application areas, including water treatment,[22] analytical chemistry,[23] nanoparticles synthesis[24,25] or surface treatments.[26,27] The low temperature plasma generated by electrical discharge, as presented by Bruggeman *et al* in their review paper in 2016,[28] can take different forms based on the method of generation, or configuration. The discharges can be ignited, for example, directly inside the liquid, or on its surface or in an aerosol.[28] Such plasmas, and their interaction with the liquid, plenty of reactive species as described by different studies.[29-31] For example, in the case of a plasma applied on water surface, hydrogen peroxide is formed through the recombination reaction of OH, produced from the water dissociation implied by the plasma/water interaction.[32,33] Others authors have shown the formation of nitrogen-based ions, like NO_2^- or NO_3^-, in case of plasma

Université de Lorraine, CNRS, IJL, F-54000 Nancy, France
**E-mail: sebastien.fontana@univ-lorraine.fr*

ignited in air at the liquid surface.[34-39] In parallel, the application of a pulsed discharge on a liquid surface can physically distort it, and leads to instabilities at the plasma/liquid interface. Pulsed discharge generates acoustic vibrations or even shock waves, whatever the pulse frequency.[40-47] Such shock waves could be used to exfoliate graphene flakes from graphite with a process similar to sonication.

In this work, a plasma process interacting with a liquid medium is used in order to exfoliate and/or functionalize graphite flakes and then develop a new method of graphene production. The functionalization of a carbon material surface corresponds to the introduction of oxygenated groups via covalent bonds. Functionalization does not make it more reactive, but the advantage is to make it less hydrophobic. This original method exhibits interesting first results. The next section presents and describes the experimental setup. The following sections deal with the plasma investigations, and the characterization of the treated graphite flakes in comparison with the raw ones.

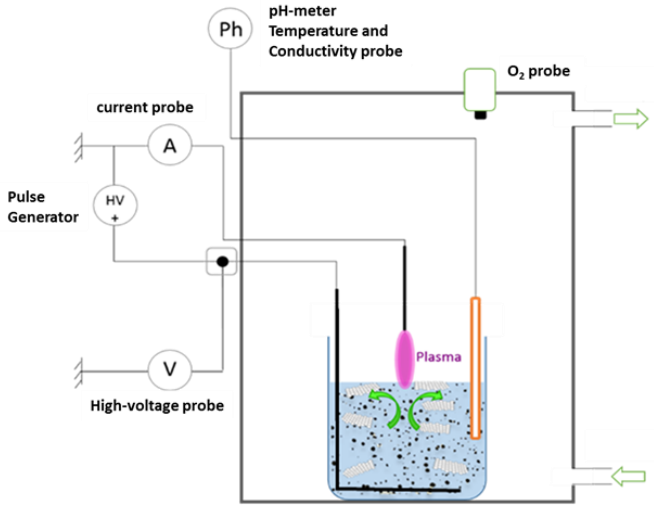

Figure 1: experimental setup for the plasma treatments.

B Experimental part

B.1 Material

The graphite used in this work is commercialized by Knano Company (Xianen, China) under the name KNG 180. The KNG 180 samples are composed of graphite nanoplatelets obtained by thermochemical process and sonication. The data sheet provided by the supplier indicates a carbon content of 99.5%wt, flake diameters between 8 and 100 µm and platelet thickness less than 100 nm. A more complete characterization of the raw KNG 180 is presented in section D of this paper. Demineralized water is used with KNG 180 nanoplatelets during the plasma treatments. Two sets of particle concentration in liquid were used in order to (i) finely study the plasma treatments of KNG 180 and (ii) produce large amount of plasma treated KNG 180. In the first case, 25 mg of KNG 180 samples were manually dispersed in 80 mL of demineralized water (0.3 $g.L^{-1}$). For the second one, 200 mg of KNG 180 were manually dispersed in 40 mL of demineralized water (5 $g.L^{-1}$).

B.2 Plasma treatments, experimental setup

Figure 1 presents the technical drawing as developed.[48]

All the experimental setup is surrounded by a hermetic box made of poly(methyl methacrylate) (PMMA). The box atmosphere can be controlled to perform the plasma treatment in different gases. Here, the chosen gas is air at atmospheric pressure. Two electrodes made of a 1 mm tungsten wire are used. The first one, a pin electrode, is set 1 mm above the liquid surface and is grounded and acts as the cathode. The second, a ring with 3 cm in diameter is immersed at the bottom of the beaker containing the liquid and acts as the anode.

Square voltage pulses are generated by a Spellman $PTV_{10}P_{350/230}$ DC generator coupled with a RLC Nanogen 1 smart HV Pulse Generator switcher. High voltage pulse amplitude, frequency and duty cycle are set at 6 kV, 6 kHz and 0.6% respectively. Throughout the plasma treatments, a Magnelab CT-D1.0-BNC current probe and a Tektronix P6015A probe are used with a LeCroy WaveSurfer 104 MXs-B oscilloscope in order to monitor the process and collect electrical data continuously. Optical emission spectroscopy is implemented in order to investigate the evolution of the chemical composition of the plasma throughout the treatment process. The plasma emission is recorded with a high-resolution spectrometer JOBIN YVON Triax 550 equipped with a 1200 $groves.mm^{-1}$ grating and an ICCD detector.

Moreover, a DeltaOhm HD2165.2 pH-meter and a DeltaOhm SP06T temperature and conductivity probe are added to the experiment to follow the main parameters of the liquid during the plasma treatment process. Due to high voltage, it is not possible to continuously collect data of pH, temperature and conductivity of the liquid. Data acquisitions are made after repetitive shutdowns of the plasma and with a step of 2 min for the first 20 minutes of treatment and 5 min beyond 20 minutes of process. The initial volume of distilled water inside the beaker is automatically maintained by a syringe pump to keep the 1 mm gap between the liquid surface and the cathode during plasma treatments. For each set of KNG 180 particles concentration in liquid, all electrical parameters remain unchanged and the plasma treatment durations are fixed at 1 hour.

After treatment, the carbon particles are recovered by freeze-drying.

B.3 Instruments and characterizations

Transmission electron microscopy (TEM) was performed on an ARM-200F apparatus at an operating voltage of 200 kV. Graphite raw particles and plasma treated samples were dispersed in absolute ethanol by sonication and were deposited on a copper grid with a holey carbon film.

Scanning electron microscopy (SEM) was carried out using a environmental Quanta FEG 650 electron microscope from the FEI Company.

X-Ray diffraction (XRD) was performed on a Bruker® D8 Advance diffractometer in the Bragg-Brentano θ/2θ configuration. The diffractometer was equipped with a molybdenum anticathode

as X-ray source ($\lambda_{MoK\alpha1}$ = 0.70930 Å). Samples were placed in Lindemann glass capillary tubes (1.5 mm inner diameter).
Thermogravimetric analyses (TGA) were performed on a Setsys Evolution 1750 Setaram® thermobalance. Two types of tests were carried out for the characterization. In the first one, the sample was heated to 1000°C with a heating rate of 2 °C/min under dry air. In the second test the thermobalance was linked to a Pfeiffer® GSD 301C Vaccum Omnistar mass spectrometer and the sample was heated under helium gas.
X-ray photoelectron spectroscopy (XPS) analyses were achieved with a Kratos Axis Ultra DLD, using an Al $K_{\alpha1}$ X-ray source (1486.6 eV). C-C and C-H bounds were taken as C_{1s} signal references at 284.6 eV. Analysed surface was of 700x300 μm^2 for 5-10 nm deep.
Raman spectroscopy investigations were performed using a LabRam HR Jobin Yvon spectrometer, with a laser wavelength of 488 nm and equipped with a microscope objective (X100). The investigations were performed on the spectral range 850-3000 cm^{-1} to detect the bands D, G, D' and 2D. The samples were dispersed in absolute ethanol and disposed on a glass plate before analysis. For all samples, five spectra were recorded to confirm their reproducibility.

C Plasma treatment characterizations

C.1 Global behaviour of the plasma treatment processes

The first set of KNG 180 concentration in liquid (25 mg of KNG 180; 80 ml of demineralized water; 0.3 $g.L^{-1}$) is implemented to allow the observation of the finest evolutions of plasma and liquid solution parameters. Indeed, in this case a change of the plasma type discharge can be observed before and after of about the first fifteen minutes of this treatment: the plasma shape and colour change drastically, from a columnar purple plasma formed firstly, to an arc/filament pink and red plasma secondly (Supplementary information Figure A). Additionally, a modification of the KNG 180 behaviour within the liquid is also noticed. Indeed, the hydrophobic nature of the graphite flakes implies a high sedimentation rate since most part of KNG 180 sample agglomerates and fall at the bottom of the beaker or stay at the liquid surface, even after the manual dispersion step. However, approximatively 15 minutes after the beginning of the treatment, the KNG 180 behaviour changes and most of the carbon flakes rise from the bottom of the beaker and progressively stay suspended in the liquid solution.
From these first observations, the KNG 180 flakes miscibility with the liquid seems improved thanks to the plasma treatment. In order to understand those evolutions and to characterize the plasma treatment, the analyses were then focused on three different aspects: the electrical pulse characterization, the plasma composition by optical emission spectroscopy and the reactive liquid evolutions (pH, temperature and conductivity).

C.2 Electrical pulse characterization

Valuable information can be extracted from electrical signals of the discharges. With high time resolution, the voltage and the current of the pulsed discharge were recorded all along the plasma treatment of the KNG 180 with the first concentration.
Figure 2 shows these electrical characteristics. Voltage signals exhibit stable and dampened oscillations at the voltage rising and falling edges, i.e. the transient regimes. These voltage oscillations are due to an impedance matching issue at the transient high frequency since the cathode is directly grounded to the electrical system. This phenomenon has repercussions on the current measurement and thus the current curves are also slightly impacted for transient measurements. Nevertheless, 250 ns after each transient regime (*i.e.* when transient amplitude is negligible), the voltage and the current measurements become reliable and reflect the real electrical characteristics of the plasma discharge. Firstly, figure 2 shows that the measured voltage differs from the set point of 6 kV, starting at 6.1 kV at the beginning of the plasma treatment and decreasing to around 5 kV at the end of the process (60 minutes). This voltage drop is due to the discharge current that increases rapidly after 10 min to reach a maximum value of about 5 A at the end of the process. The power generator reaches its operating limits: the system is not able to maintain the 6 kV constant voltage for such high current density during the pulse duration. The use of a more powerful high voltage generator could address this technical issue.

ARTICLE

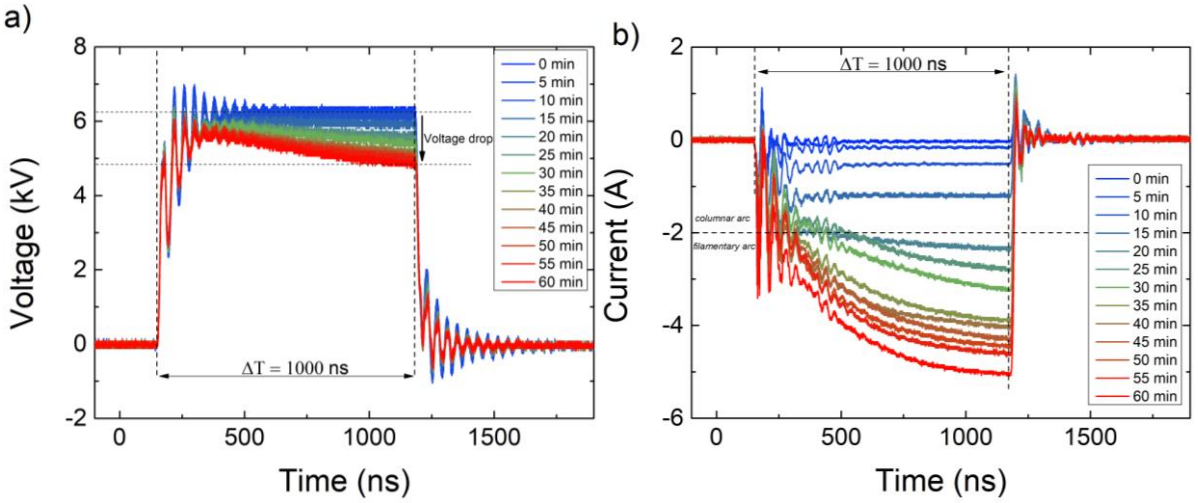

Figure 2: chronogram of (a) the voltage and (b) the current during the plasma treatment of 25 mg of KNG 180 sample in 80 mL of water and in air gas.

Secondly, the shape of the discharge current changes during the plasma treatment. The current curves have a square shape from the beginning to the end of each voltage pulse before about 15 min of treatment. Beyond this plasma treatment period and with a discharge current value of around 2 A, the initial square shape of the current changes to an exponential decay shape, which also corresponds to a change in the plasma aspect with filamentary discharges. Indeed, the current equation refers to a charging system and could be writen as follow:

$$i(t) = I_a.(1 - e^{-t/\tau})$$

where I_a is the value of the current limit (asymptotic value of the current measurement) whose value depends on the voltage and τ is the time constant of a RC circuit. Based on these electrical characteristics, the pulse power (mean power during the 1 µs plasma discharge) and the mean power (continuous process power consumption) evolutions with the process time of the KNG 180 plasma treatment were determined (figure 3).

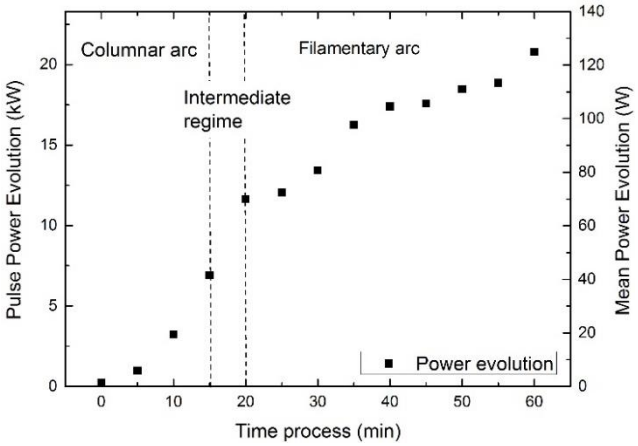

Figure 3: pulse power and the associated mean power evolutions during the plasma treatment process of 25 mg of KNG 180 in 80 mL of water and in air gas.

At the early beginning of the process and until the intermediate plasma regime previously described (between 15 to 20 minutes), the pulse power increases rapidly. This first power evolution occurs when the plasma discharge remains stable during the columnar arc discharge regime. Beyond the intermediate plasma regime and after 20 min of process, the pulse power evolves differently and exhibits wavy variations with time, which correspond to the occurrence of filamentary arc discharges. For this first set of KNG 180 plasma treatment, the mean power reached a maximum value of 125 W. It should be noted that in this case the power consumption throughout a 1h process is then of

73 W, which corresponds to 2.92 $kW.g^{-1}$ in order to treat the initial 25 mg of KNG 180 sample.

C.3 Plasma composition

In the present case, arc discharges are fleeting and tinny types of plasma that are difficult to study due to the need of spatially and temporally resolved diagnostic tool. Nevertheless, it is possible to determine the presence of some plasma species, spatially and temporally integrated, thanks to optical emission spectroscopy (OES). Of course, OES gives a partial view of the different plasma species: only excited radiative species can be identified by OES.

Figure 4 shows the evolution of the plasma emission spectra with the processing time. In order to better understand the evolution of the plasma treatment process itself, two emission spectra taken at 5 min and 40 min process time are also extracted from the emission spectra chronograph. As expected from the previous electrical results, some important evolutions can be observed throughout the process time. Globally, the band assignment of the emission spectra indicates the presence of numerous molecular nitrogen bands, different bands associated with the OH molecules, and lines from O and H atoms. During the first fifteen minutes of the treatments, based on the evolution intensity of the recorded emission spectra, molecular nitrogen emission bands remain the most intense, with some oxygen and hydrogen emissions lines. At this step, successive plasma discharges occur in an air mainly composed of nitrogen, oxygen and some water vapour. The extracted plasma emission spectrum at 5 min confirms the nature of the air plasma and corresponds to the purple columnar discharges (see supplementary information Figure A). Also, the observation of strong molecular nitrogen bands in the plasma could imply the presence of highly reactive nitrogen species that can interact with the liquid solution and lead to the formation of numerous nitrogen containing chemical species.[28, 33-39]

However, starting to around fifteen minutes and beyond, the plasma signature changes drastically. An important rise in intensity of OH bands and H and O lines occurs and they become more intense than the nitrogen emission bands. These species can be associated to by-products of water dissociation (O, H, or OH). This can be interpreted as an indication of a transition from a plasma ignited in an ambient air (i.e. air with traces of water vapour) at the beginning of the treatment to a plasma ignited in an atmosphere mainly composed of water vapour with residual air. The presence of a high concentration of water vapour in the gas phase can be linked to the evaporation of the liquid solution due to its heating. This result remarkably coincides with the observed change of the discharge current shape and with the experimental observation of the transition from a columnar arc plasma to a filamentary arc plasma that occurs after fifteen minutes of plasma treatment of the KNG 180. OH bands and H and O lines reach a maximum intensity after forty minutes of treatment, as it could be observed on the extracted plasma emission spectrum at 40 min (figure 4). These emission intensities remain constant for the rest of the plasma treatment. Again, the presence of these emissive species coming from the plasma discharge could interact with the liquid solution containing the KNG 180 particles. Nonetheless, no carbon-containing species (e.g. CO, CN or CH) are observed in spectra throughout the plasma treatment, even with the high current pulse observed at the end of the treatments. The absence of these radiative species could be interpreted as a no degradation of the graphitic layer of the KNG 180 particles leading to a plasma process which induces very low defect in the carbon planes.

C.4 Reactive liquid evolution

Figure 5.a shows the variation of the reactive liquid pH with the processing time. As expected for demineralized water, the initial pH is around 8. During the columnar arc discharges and before 15 minutes of the process, the pH of the solution decreases rapidly down to a value around 3.6. It should also be noted that the maximum pH variation occurs between 5 and 10 min. During the intermediate plasma regime, the pH value of 3.6 is almost constant. Beyond 20 minutes the pH value decreases again but at a lower rate to reach a final value of 2.8 at 60 minutes. This evolution clearly indicates a change in the liquid nature with a strong acidification of the solution. This acidification is likely due to new species issued from the interaction of the plasma with the liquid. Indeed, many chemical reactions occur inside the plasma volume or at the plasma-liquid interphase that could explain this evolution. Although the plasma-liquid interaction is still a topic of studies, some species have already been identified in the plasma-liquid interaction for similar experiments. Some authors observed the formation of different nitrogen-containing chemical species when the plasma is ignited in air, and they assigned the liquid acidification to species like NO_2^- for example.[33-39]

ARTICLE

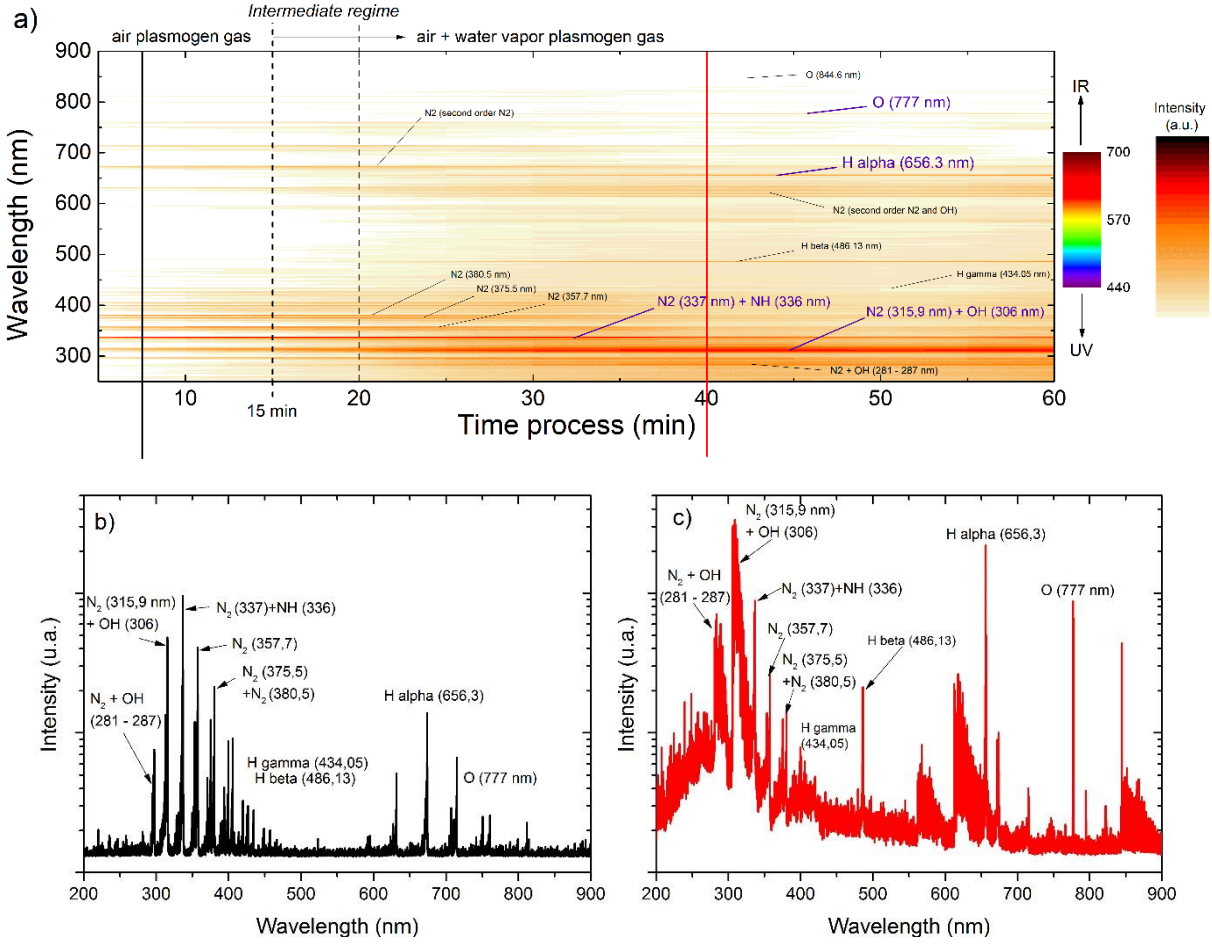

Figure 4: (a) chronograph of the plasma emission spectra along the plasma treatment of 25 mg of KNG 180 in 80 mL of water and in air; (b) plasma emission spectrum of air at 5 min treatment; (c) plasma emission spectrum of air with major water

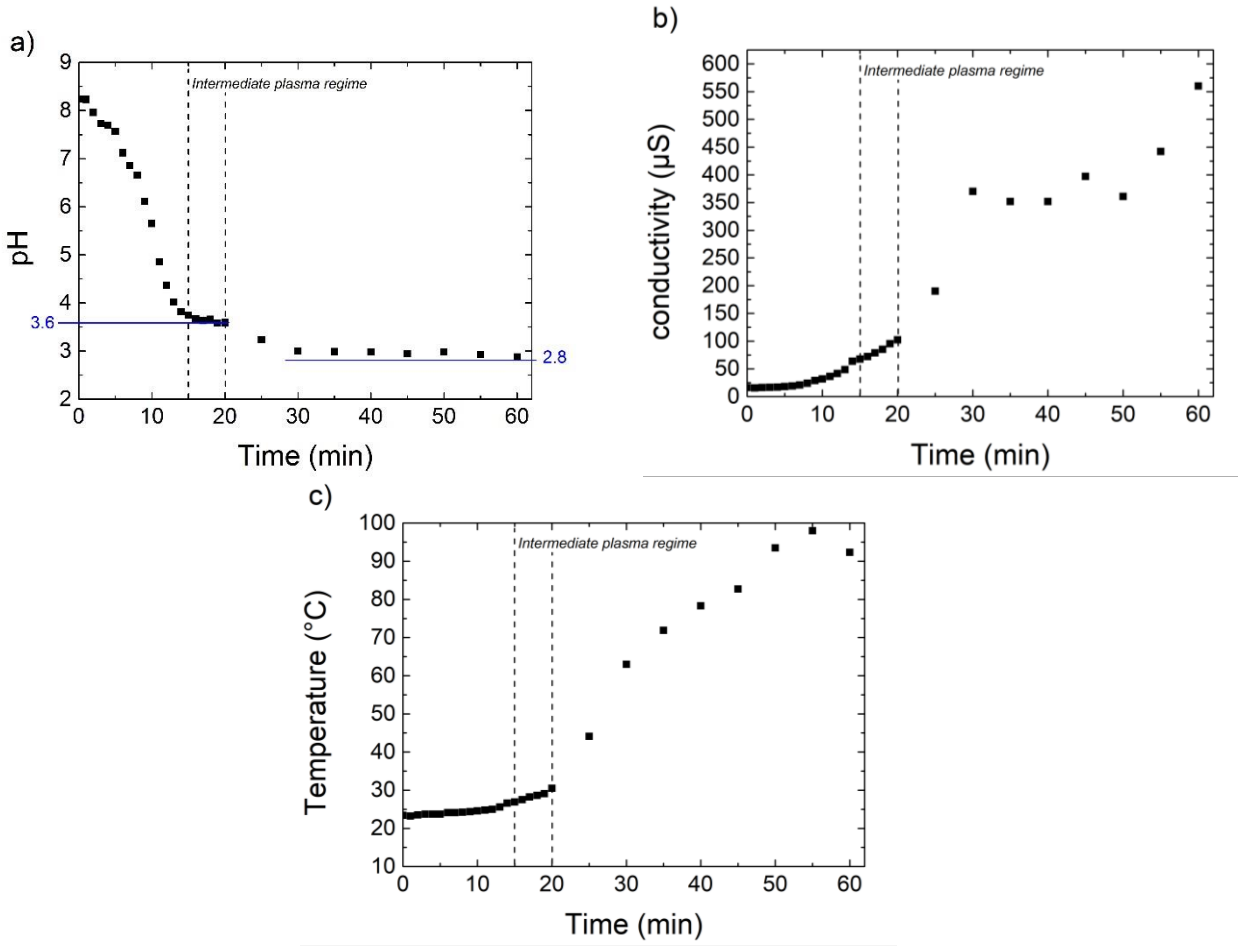

Figure 5: time evolution of the liquid (a) pH, (b) conductivity, (c) temperature with the processing time of 25 mg of KNG 180 in 80 mL of water and in air. The intermediate plasma regime is identified in each case.

This possibility is consistent with the OES results described above since for the first fifteen minutes the treatment mainly occurs in an air plasma. After a dissolution inside the reacting liquid at the plasma liquid interface, the presence of those species could explain the sharp fall of pH observed in figure 5. Beyond the intermediate plasma regime, around 15-20 minutes, the water vapour in the plasma volume becomes significant, and could imply the formation of H_2O_2 and hydrated H^+ due to the formation and degradation of the water vapour, as observed by other authors.[32,33]

At the same processing time (starting to 15 min), it is also worth noting that acidification of the solution gets slower as the plasma switches from columnar to filamentary discharges, which also corresponds to the rise of the dispersion of carbon particles in the solution. All these results lead to link the three phenomena together.

The evolution of the reactive liquid conductivity with process time is shown in figure 5.b. As expected, the demineralized water has a low conductivity with value of 10 µS.cm^{-1} at the beginning of the treatment. This conductivity remains very low during the first 10 minutes of the treatment. After 10 minutes, the conductivity rapidly increases until the end of the KNG 180 sample treatment, and reaches a final value of about 450 µS.cm^{-1}. This transition at about 10 minutes seems to be correlated with the high pH variation that also intervenes at the same time during the plasma treatment. Furthermore, the conductivity evolution and discharge current evolution in figure 3 match together since the more the liquid solution conductivity increases, the higher the discharge current. Ditto with regard to the levels of conductivities and currents measured beyond 30 minutes, which reach values comprised between 350 and 450 µS.cm^{-1} and between 3 and 5 A, respectively. The dispersion of graphite that exhibits a high electrical conductivity and the formation of new chemical species, especially ionic species, could also explain the increase of the conductivity observed after 10 minutes.

Figure 5.c shows the temperature evolution of the reactive liquid with the processing time. As for the other liquid parameters, the temperature evolution can be divided into three major parts. For the first one, between the beginning of the treatment and until 15 minutes (columnar arc plasma), the temperature remains stable (around 25 °C, the room temperature). A slight rise in temperature is measured secondly between 15 and 20 minutes processing time, which could be due to the fast evolution of the discharge current during the intermediate plasma regime. After 20 minutes and in a filamentary plasma discharge regime, the temperature increases rapidly to reach almost 90-100 °C at the end of the plasma treatment. The rise of the liquid conductivity coupled to the intense and filamentary arc discharges imply a fast

increase of the liquid temperature at the plasma/liquid interface by Joule effect. The graphite dispersion and the resulting convection inside the beaker should also help the liquid heating. Both the filamentary plasma regime and the rapid rise of the liquid temperature could explain the important evaporation and degradation of the water molecules that is observed by OES at about 15 minutes of treatment and beyond.

The different results of both the pulsed plasma and the liquid characterizations give some clues in order to make hypothesis on the physico-chemical mechanisms that occur during the KNG 180 plasma treatment. In the first step of the treatment (until 15 minutes), an air plasma is essentially formed at the liquid surface, which implies the formation of some chemical species that increase the liquid acidity. A columnar arc plasma then takes place at the liquid surface. At some point, in our case for a pH of about 3.6, the liquid solution with KNG 180 particles reaches a limit condition leading to the increase of the liquid conductivity. The discharge is still columnar but the discharge current starts rising. A cascading phenomenon starts to take place between 15 -20 min, leading to an intermediate plasma discharge regime: an important increase of the discharge current induces an increase in the liquid temperature. Consequently, the composition of the plasma gas changes as well, which make *in fine* a better dispersion of KNG 180 for an increase of the liquid conductivity. With the conductivity evolution, the electrical pulse current reaches higher values and implies the formation of filamentary more intense plasma and more numerous and much dispersed graphitic particles inside the liquid volume as well. Beyond 20 min, the filamentary plasma regime is definitively reached and liquid parameters as conductivity and temperature continue to increase until the end of the plasma treatment while the pH tends slowly to a value of 2.8.

It is important to note that the rise in temperature at the plasma/liquid interface implies producing more and more water vapour. New emission bands are observed due to the water dissociation, which indicates the formation of new chemical species with oxidizing properties. In these conditions, it is important to understand that the plasma treatment leads to the formation of chemically reactive species, shock waves and heat, that could imply major modifications of the pristine KNG 180 graphite flakes.

C.5 Second process analysis

In order to allow a much larger production of plasma treated KNG 180, the second set of KNG 180 concentration in liquid (200 mg of KNG 180; 40 mL of demineralized water; 5 $g.L^{-1}$) is implemented. In doing so, it is essential to ensure that the reaction mechanisms remain the same as with the first set of KNG 180 concentration in liquid. From an observational point of view and as in the previous set, a change of the plasma type can be observed but much earlier. The switch from a columnar purple plasma to a filamentary pink and red arc plasma takes place only 5 minutes after the beginning of the KNG 180 plasma treatment. Like in the first set, OES was used to characterize and to monitor the plasma composition evolution (figure 6). The band assignment still indicates the presence of a majority of nitrogen bands at the very beginning of the plasma treatment, before 5 minutes. However, bands ascribed to OH, O and H appear very early and intensively beyond this time. The evolution of the plasma composition still exhibits the transition from an air plasma to a majority water vapour plasma. Only the transition from columnar to filamentary arc discharge is faster and occurs in the first five minutes of the process.

The recorded electrical signals of the plasma discharges for the second operating mode given in figure 7 are in accordance with the OES measurements since the change of the current curve shape, from square to an exponential evolution decay, takes place in the first ten minutes of treatment. It should also be noted that a more important drop of the discharge high voltage is recorded with a minimal value of about 3.5 kV at the end of the voltage pulse at 60 minutes of treatment. Nevertheless, the breakdown voltage and the established voltages seem sufficient to initiate and to sustain the plasma discharge, respectively.

Based on the electrical characterization and as previously defined, the pulse power and the mean power evolution for this second set were determined (Supplementary information Figure B). The powers present a rapid increase in the first ten minutes of process and reach values of 20 kW and 120 W for pulse power and mean power, respectively. The maximum mean power reached a maximal value of 147 W at 20 minutes of process.

Beyond 20 minutes, this value progressively decreases to 120 W. Once again, this drop in power is due to the limitation of the power generator and capacity storage already mentioned. The power consumption throughout a 1h process is then of 116 W that correspond to 580 $W.g^{-1}$ in order to treat the initial 200 mg of KNG 180, thus an increase in the energy efficiency of the plasma treatment process by a factor of about 5 compare to the first set treated.

The second operation mode shows that a rise in the carbon concentration implies an acceleration of the process that can be used to produce larger quantity of treated carbon without changing the plasma characteristics, which therefore cannot change the reactional mechanisms occurring at the plasma/ liquid interface. The next part of this work focuses on the characterization of the modified KNG 180 samples using the second set of KNG 180 concentration in liquid during the plasma treatment.

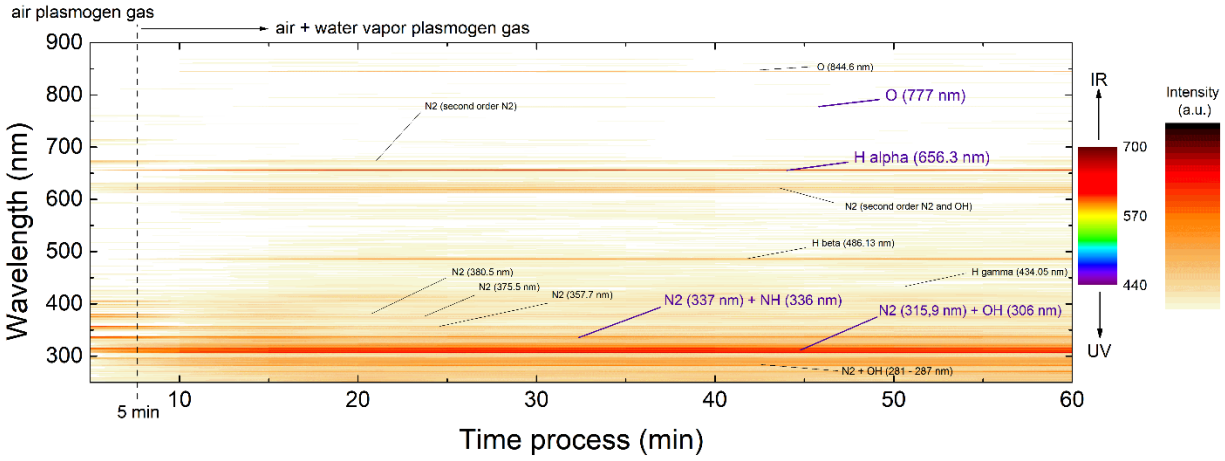

Figure 6: chronograph of the plasma emission spectra during the treatment of 200 mg of KNG 180 in 40 mL of water and in air.

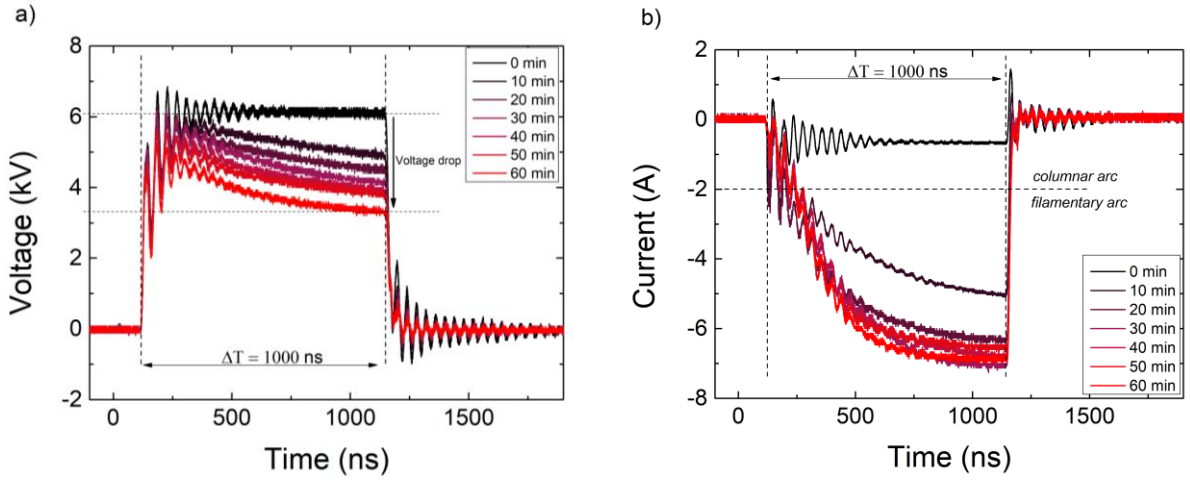

Figure 7: chronogram of (a) the voltage and (b) the current during the plasma treatment of 200 mg of KNG 180 sample in 40 mL of water and in air.

D Graphite flakes characterization

Pristine KNG 180 and plasma treated KNG 180 samples were studied by XRD, TGA, Raman spectroscopy and XPS. The KNG 180 plasma sample treated with the second protocol (200 mg) was lyophilised before characterization to extract the remaining water and to avoid as much as possible the re-stacking of the separated graphene layers. It is interesting to note that after the plasma treatment and the lyophilisation, the treated sample presents a higher compatibility with water, as shown figure 8. The plasma treated sample remains dispersed in distilled water for more than 6 hours, compared to the initial KNG 180, highly hydrophobic, that exhibits a higher sedimentation in the first 5 minutes.

Figure 9 shows SEM and TEM micrographs of both samples, before and after the plasma treatment. Thin graphite flakes are observed for both samples, with a large size distribution from a few µm to more than 25 µm. In both cases, the flakes exhibit a high aspect ratio. The pristine KNG 180 particles show well define edges; small amounts of amorphous carbon are also observed. In the treated sample, partial exfoliation of the graphitic structure is revealed since the particles appear quite thinner. As pristine sample, they also present clean edges, without visible defect that could be expected after the plasma treatment. However, a slight pollution that can be due to some tungsten oxide from the submerged electrode of the sample is observed.

SEM and TEM micrographs do not give enough information to clearly identify the effect of the plasma treatment, but indicate that no important defect was generated since the aspect of the graphite particles does not change. Moreover, it is noteworthy that SEM and TEM providing only local data on a very small proportion of the sample, these results are not sufficient to define the general trend concerning the treatment effect on the graphite structure.

Figure 8: evolution of the graphite dispersion (5 g.L^{-1}) in demineralized water after sonication for the treated sample (left bottle) and initial KNG 180 (right bottle), after a) 0 minutes, b) 5 minutes, c) 1 hour.

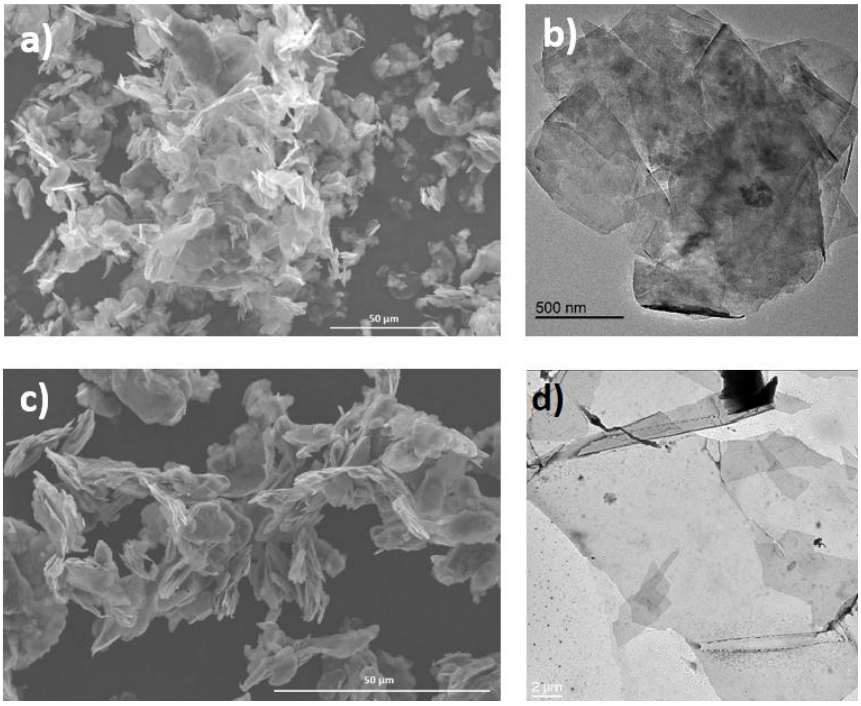

Figure 9: SEM and TEM micrographs of the KNG 180 untreated (a) and b)) and treated by plasma (c) and d)).

X-ray diffraction pattern of untreated and plasma treated samples show only graphite reflexions (Supplementary information Figure C). From the width of the (002), (004) and (006) Bragg peaks attributed to hexagonal graphite, it is possible to determine the crystallite size along the c axis, noted L_c, and the number of stacked graphene layers. It also possible to determine the strain, note ε, induced in powders du to crystal distortion. The calculation is performed using the Williamson-Hall method.

$$\sqrt{\beta_{mes}^2 - \beta_{ins}^2} * cos\theta = \frac{0.9 * \lambda_{Mo}}{L_c} + 4\,\varepsilon\, sin\theta$$

with θ the Bragg angle of the diffraction peak, and β_{mes} the full-width at half maximum (FWHM) of the corresponding Bragg peak. This value is corrected by β_{ins}, due to the instrument broadening.

Table 1: Crystallite size and strain along the c axis and number of graphene layers

	untreaded sample	plasma treated sample
L_c (nm)	19.4	13.9
Number of graphene layers	58	42
Strain ε	0.0008	0.001

The pristine KNG 180 shows a value of L_c around 19.4 nm and the treated sample around 13.9 nm. With two graphene layers separated by a 0.335 nm d-spacing, an estimation of the layer stacking can be done, which leads to 58 layers for the untreated KNG 180 and around 42 layers for the plasma

treated samples. As expected, the number of stacked graphene layers decreases with the plasma treatment, by 25% in the present case. The X-ray diffraction results indicated a partial exfoliation of the graphite flakes with a diminution of the number of graphene layers. Moreover, the strain ε increases very slightly in the case of the treated sample.

To complete this structural study and to check the presence of turbostratic structure, both samples were characterized by Raman spectroscopy. Raman spectroscopy is one of the most common technique used to characterize carbon materials. In the case of graphite, four major features are expected: the G band around 1580 cm^{-1}, the D band, around 1350 cm^{-1}, the D' band around 1620 cm^{-1}, and 2D around 2700 cm^{-1}.[49-51] The G band, which occurs for all graphitic structures, represents the in-plane band stretching motion of sp^2 atoms. The D band on the other hand is associated with the breathing modes of the C_6 carbon rings.[49-51] The D band intensity can be correlated to the amount of the structural defects occurring inside the graphite structure. The classical solution to estimate the evolution of the defect density is to observe the evolution of the D to G band intensity ratio, noted I_D/I_G.[49-51] The D' band can be observed in case of disordered stacking, and is correlated to the D band intensity. Finally, the 2D band, an overtone of the D band, is related to the stacking order of the material. The shape of the band evolves with the number of stacked graphene layers, a single graphene layer will show a single sharp Lorentzian peak for example. The peak shape evolves with the number of layers to become similar to the graphite one for five or more layers, with two Lorentzian components, respectively around 2660 cm^{-1} and 2740 cm^{-1}. In case of turbostratic graphite, a third Lorentzian component appeares around 2710 cm^{-1}.[51-54] Raman spectra of both samples are shown in figure 10. Both spectra are normalized with respect to the G band intensity. The pristine KNG 180 shows an I_D/I_G ratio of 0.11, which indicates the presence of few defects in the graphite structure.

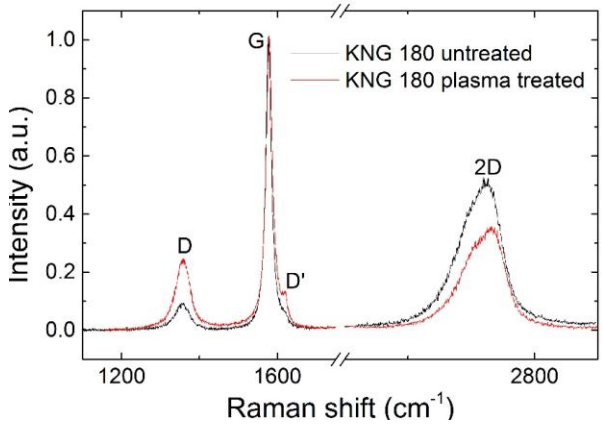

Figure 10: Raman Spectra (λ = 488nm) of the KNG 180 untreated sample (black) and treated by plasma (red).

The 2D band can be fitted with three Lorentzian components; two components were attributed to the hexagonal graphite and one to the turbostratic graphite (Supplementary Information Figure D and E). The Lorentzian component associated with the turbostratic graphite remains low in intensity and represents only 10% of the 2D band integrated intensity. The treated sample also exhibits the four main bands, with a few variations. First, a rise of the normalised intensity of the D band is observed, with an I_D/I_G ratio reaching 0.23. This value, higher than that of pristine sample reveals a small increase in defect density inside the graphitic structure, in agreement with the strain measured by XRD. The other evolution is a decrease in the normalised intensity of the 2D band, but at the same time, a rise of its turbostratic component part is observed. This evolution could indicate a decrease in the hexagonal graphite fraction of the material in favour of the turbostratic stacking.

Thermogravimetric analysis under dry air was performed to analyse the purity of the samples, and their thermal stability. Figure 11 shows the weight loss between room temperature and 1000 °C and the derivative curves for pristine and treated samples. Both materials present a final mass loss less than 100%. The ash content of the pristine KNG 180 represents 2.5%. This value is higher than what should be expected for a commercial graphite. On the other hand, the residue after combustion of the treated sample reaches 10%, which can be explained by a tungsten pollution from the submerged electrode degraded by the treatment. The pristine KNG 180 sample shows a major weight loss between 500 and 775 °C, with a maximum around 700 °C. The treated sample combustion starts around 500 °C with a maximum weight loss around 675 °C and ends around 775 °C, as the pristine sample. The maximum combustion rate is observed at lower temperature than for untreated sample, which indicates thinner particles. This result is in good correlation with Raman spectroscopy and X-ray diffraction results.

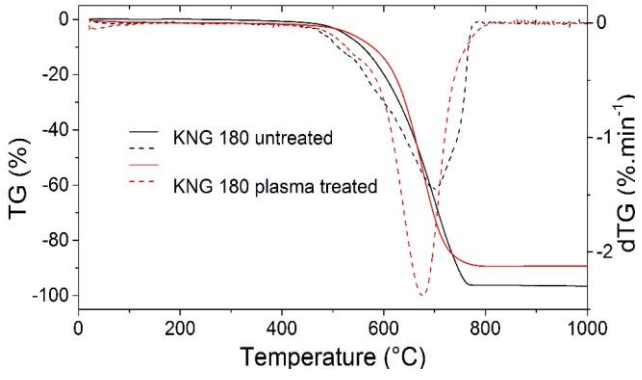

Figure 11: TGA Thermograms (under dry air) of the KNG 180 untreated sample (black) and treated by plasma (red).

As shown by the sedimentation rate, the carbon/water interactions are modified by the plasma treatment. This is presumably due to a chemical modification of the surface of the graphitic particles, leading to an evolution of the carbon/water compatibility. In order to confirm the changes in the chemical properties, both samples were analysed by thermogravimetric analysis under dry helium coupled with mass spectrometry. Two mass spectrometry signals were studied during the thermal decomposition: carbon monoxide (m/z = 28) and carbon dioxide (m/z = 44).

The thermograms and mass spectrometry signals for both samples are shown in the supplementary information (Figures E and F). The pristine KNG 180 sample exhibits a 0.25% mass loss around 100 °C correlated to a water release. The presence of water can easily be explained by its adsorption on the surface of the graphite flakes. Another constant and low weight loss is observed from 200 °C until the end of the test that represents around 1.5% of the sample weight. This weight loss is correlated with a CO emission, between 200 and 350 °C, and a CO_2 emission between 300 and 700 °C. Those emissions indicate the presence of some oxygen-functions on the surface of the graphite flakes, mostly carbonyl and carboxyl groups.

As the pristine one, the plasma treated sample shows a first weight loss around 100 °C, which can also be associated to the water adsorbed on the sample. The second weight loss that starts around 200 °C, is more important, with a final weight loss higher than 3.5%; it is in good correlation with two CO gas emissions, respectively between 200 and 350 °C for the first one, and 500 to 650 °C for the second one, and a CO_2 emission between 450 and 650 °C. Those gas emissions are due to oxygen-functions present on the graphite surface. The emission between 200 and 350 °C can easily be attributed to carboxyl groups, and the emission between 500 and 650 °C to carbonyl groups. The functionalization of the carbon surface by the plasma treatment is then confirmed and explains the modification of the expected carbon/water interactions. This functionalization is consistent with the increase in the defect density observed by Raman spectroscopy after the plasma treatment.

To go further, XPS analyses were performed on pristine and plasma treated KNG 180 samples. The corresponding C_{1S} spectra are given figure 12. The curve fitting of the C_{1S} spectrum of the pristine KNG 180 shows four types of bondings, the C=C (≈284.6 eV) that logically corresponds to the most intense peak, the C-C (≈285.1 eV), the C-H (285.6 eV) and the C-OH (286.6 eV) with a really low intensity. This deconvolution agrees with the low level of oxidation observed by TGA coupled with mass spectrometry.

The decomposition of the C_{1S} spectrum of the plasma treated sample shows the presence of the same four bands, with an increase in the intensity of the C-H and C-OH peaks, and two new bands corresponding to C=O (≈ 288.3 eV) and O-C=O (289.1 eV). This spectrum confirms the formation of new oxygen-functions on the graphite surface due to the plasma treatment, and agrees with the formation of carbonyl and carboxyl groups. The use of several complementary techniques demonstrate that the plasma treatment (formation of shockwave, chemical modification of the liquid…) applied on the KNG 180 graphite sample leads to a partial exfoliation of the graphite structure with a diminution of the number of graphene layers. In addition, a part of the hexagonal structure is replaced by a turbostratic one with a random organisation along the c-axis, as observed by Raman spectroscopy. This exfoliation is coupled with a chemical modification of the graphite flakes, with the formation of carbonyl and carboxyl groups, observed by TGA under dry helium coupled with mass spectrometry and XPS.

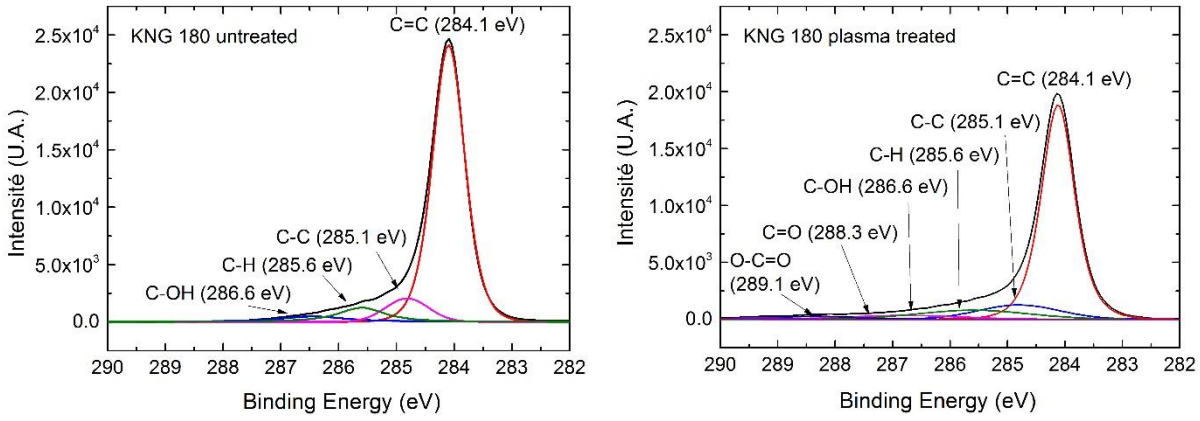

Figure 12: XPS C (1s) decomposed spectrum of the KNG 180 untreated sample and treated by plasma.

Conclusions

In this work plasma ignited on liquid was used to modify graphite particles, with a partial exfoliation and moderate functionalization. The plasma treatment can be divided in two steps. First, a blue columnar nitrogen plasma is formed and leads to a strong acidification of the liquid, due to the formation of different nitrogen-containing chemical species.

In this first step, the graphite flakes present a rise of their dispersion inside the liquid. An increase of the discharge current is also observed. When the current reaches about 2 A, the discharge evolves to a water vapour pink arc/filament plasma. The plasma treatment leads to the formation of chemical species shock and heat that are used to modify the graphite flakes.

The characterization of untreated and treated graphite samples highlights a partial exfoliation with a 25% decrease in the flakes thickness and the formation of some turbostratic graphene planes stacking. The plasma treatment also leads to a slight oxidation of the surface of the graphitic particles with the formation of carbonyl and carboxyl chemical groups. The exfoliation implies the formation of small structural defects compared to conventional chemical treatments. And the functionalization favours the dispersion of the flakes in aqueous media.

Consequently, the use of plasma in liquid media can be considered to produce graphite nanoparticles and graphenic materials more quickly and with less defaults in comparison with the techniques currently used. Further research is needed for a better understanding of the process and a better control of the exfoliation. In addition, the effects of pulse properties, reactive liquid and initial atmosphere should also be investigated.

Conflicts of interest

There are no conflicts to declare.

Acknowledgements

The authors would like to thank L. Aranda from Institut Jean Lamour for his assistance in thermogravimetric analysis, and A. Renard from Laboratoire de Chimie Physique et Microbiologie pour les Matériaux et l'Environnement for his careful XPS measurements.

References

1 C. Lee, X. Wei, J. W. Ksyar and J. Hone, *Science*, 2008, **321** (5887), 385-387.
2 Y. Zhu, S. Murali, W. Cai, X. Li, J. W. Suk, J. R. Potts, R. S. Ruoff, *Advanced materials*, 2002, **22** (35), 3906-3924.
3 A. A. Balandin, S. Ghosh, W. Bao, I. Calizo, D. Teweldebrham, F. Miao and C. N. Lau, *Nano Lett.*, 2008, **8**, 902-907.
4 M. Stoller, S. Park, Y. Zhu, J. An and R. Ruoff, R., *Nano Lett.,* 2008, **8**, 3498-3502.
5 R. Nair, P. Blake, A. Grigorenko, K. Novoselov, T. Booth, T. Stauber, N. Peres and A. Geim, *Science*, 2008, **320** (5881), 1308-1308.
6 A. Reina, X. Jia, J. Ho, D. Nezich, H. Son, V. Bulovic, M. Dresselhaus and J. Kong, *Nano Letters*, 2009, **9**(1), 30-35.
7 G. M. Rutter, J. N. Crain, N. P. Guisinger, T. Li and J. A. Stroscio, *Science*, 2007, **317** (5835), 219-22.
8 V. Chandra, J. Park, Y. Chun, J. Lee, I. Hwang and K. Kim, *ACS Nano*, 2010, **4**(7), 3979-3986.
9 S. C. O'hern, M. S. H. Boutilier, J. C. Idrobo, Y. Song, J. Kong, T. Laoui, M. Atieh, R. Karnik, *Nano Letter*, 2014, **14**, 1234.
10 Y. Zhu, S. Murali, M. D. Stoller, K. J. Ganesh, W. Cai, P. J. Ferreira, A. Pirkle, R. M. Wallace, K. A. Cychosz, M. Thommes, D. Su, E.A. Stach, R.S. Ruoff, *Science*, 2011, **332**, 1537.
11 C. Tan, J. Rodriguez-Lopez, J. J. Parks, N. L. Ritzert, D. C. Ralph, H. D. Abruna, *ACS Nano*, 2012, **6**, 3070.
12 B. Z. Jang and A. Zhamu, *Journal of Material Science*, 2008, **43**, 5092-5101.
13 K. Novoselov, A. K. Geim, S. V. Morozov, D. Jiang, Y. Zhang, S. V. Dubonos, I. V. Grigorieva and A. A. Firsov, *Science*, 2004, **306**(5696), 666-669.
14 H. L. Poh, F. Sanek, A. Ambrosi, G. Zhao, Z. Soferb, and M. Pumera, *Nanoscale*, 2012, **4**, 3515.
15 D. C. Marcano, D. V. Kosynkin, J. M. Berlin, A. Sinitskii, Z. Sun, A. Slesarev, L. B. Alemany, W. Lu, and J. M. Tour, *ACS Nano*, 2010, **4**, 4806-4814.
16 V. Panwar, A. Chattree and K. Pal, *Physica E*, 2015, **73**, 235-241.
17 P. Turner, M. Hodnett, R. Dorey and and J. D. Carey, *Scientific Reports*, 2019, **9**, 8710.
18 J. C. Shelton, H. R. Patil and J. M. Blakely, 1974, *Surface Science*, **43** (2), 493-520.
19 K. S. Kim, Y. Zhao, H. Jang, S. Y. Lee, J. M. Kim, J. H. Ahn, P. Kim, J. Y. Choi and B. H. Hong, *Nature*, 2009, **457** (7230), 706-710.
20 J. C. Hamilton and J. M. Blakely, *Surface Science*, 1980, **91** (1), 199-217.
21 S. Chae, M. Bratescu and N. Saito, *J. Phys. Chem. C*, 2017, **121**(42), 23793-23802.
22 J. E. Foster, B. S. Sommers, S. N. Guker, I. M. Blankson and G. Adamovsky, *IEEE trans. Plasma Science*, 2012, **40**, 1311-1323.
23 M. R. Webb and G. M. Hieftje, *Anal. Chem.*, 2009, **81**, 862-867.
24 M. Smoluch, P. Mielczarek and J. Silberring, *Mass Spectrometry Reviews*, 2016, **35**, 22-34.
25 D. Mariotti, J. Patel, V. Svrcek and P. Maguire, *Plasma Proc. Polym.*, 2012, **9**, 1074-85.
26 T. Ishijima, K. Nosaka, Y. Tanaka, Y. Uesugi, Y. Goto and H. Horibe, *Applied Physics letters*, 2013, **103**, 142101.
27 J. F. Friedrich, N. Mix, R. D. Schulze, A. Meyer-Plath, R. Ranjit joshi and S. Wettmarshausen, *Plasma proc. Polymer*., 2008, **5**, 407-423.
28 P. J. Bruggeman, M. J. Kushner, B. R. Locke, J. G. E. Gardeniers, W. G. Graham, D. B. Graves, *et al.*, *Plasma Sources Science and Technologies*, 2016, **25**, 053002.
29 W. M. Deen, Analysis of transport phenomena, 2012, New York: Oxford University press.
30 S. R. De Groot and P. Mazur, Non-equilibrium thermodynamics 2011, New York: Dover Publications.
31 B. C. Garette, G. K. Schenter and A. Morita, *Chemistry Review*, 2006, **106**, 1355-74.

32 P. Lukes, E. Dolezalova, I. Sisrova and M. Clupek, *Plasma Sources Science and Technology*, 2014, **23**, 015019.
33 B. Locke and P. Lukeš, *Special issue: Plasma and Liquids. Plasma Processes and Polymers*, 2018, **15**(6), 243-308.
34 F. Liu, P. Sun, N. Bai, Y. Tian, H. Zhou, S. Wei, Y. Zhou, J. Zhang, W. Zhu, K. Becker and J. Fang, *Plasma Processes and Polymers*, 2010, **7**(3-4), 231-236.
35 K. Oehmigen, T, Hoder, C. Wilke, R. Brandenburg, M. Hahnel, K. Weltmann and T. von Woedtke, *IEEE Transactions on Plasma Science*, 2011, **39**(11), 2646-2647.
36 K. Oehmigen, M. Hähnel, R. Brandenburg, C. Wilke, K. Weltmann and T. von Woedtke, *Plasma Processes and Polymers*, 2010, **7**(3-4), 250-257.
37 M. Pavlovich, T. Ono, C. Galleher, B. Curtis, D. Clark, Z. Machala and D. Graves, *J. Phys. D: Appl. Phys.*, 2014, **47**(50), 505202.
38 M. Pavlovich, D. Clark and D. Graves, *Plasma Sources Science and Technology*, 2014, **23**(6), 065036.
39 R. Burlica, R. Grim, K. Shih, D. Balkwill and B. Locke, *Plasma Processes and Polymers*, 2010, **7**(8), 640-649.
40 J. Zeleny, *Phys. Rev., 1917,* **10**, 1-6.
41 J. R. Melcher and C. V. Smith C.V., *Phys. Fluids*, 1969, **12**, 778.
42 T. B. Jones and G. W. Bliss, *Journal of Applied Physics*, 1977, **48**, 1412.
43 P. K. Waston, *IEEE Trans. Ind. Appl.*, 1985, **EI-20**, 396.
44 M. Hase, S. N. Watannabe and K. Yoshikawa, *Phys. Rev.*, 2006, **E74**, 046301.
45 S. Korobeinikov, A. V. Melekhov, Y. N. Sinikh and Y.G. Soloveichik, *High Temperature*, 2001, **39**, 368.
46 P. J. Bruggenam, L. M. Graham, J. Degroote, J. Vierendeels and C. Leys, *J. Phys. D: Appl. Phys*, 2007, **40**, 4776-86.
47 T. Sugimoto and Y. Higashiyama, *J. electrostat.*, 2001, **2001**, 219.
48 S. Cuynet, M. Ponçot, S. Fontana, A. Letoffé, T. Belmonte, G. Henrion, C. Hérold, I. Royaud, 2020, Patent number FR2002479.
49 F. Tuinstra and L. Koenig, *J. Chem. Phys.,* 1970, **53**, 1126-30.
50 R. J. Nemanich and S. A. Solin, *Phys. Rev.*, 1979, **20**, 392-401.
51 A. C. Ferrari J.C. Meyer, V. Scardaci, C. Casiraghi, M. Lazzeri, F. Mauri, S. Piscanec, D. Jiang, K. S. Novoselov, S. Roth, and A. K. Geim, Phys. Rev. Lett., 2006, **97**, 187401.
52 R. P. Vidano, D. B. Fischbach, L. J. Willis and T. M. Loehr, *Solid State Comm.*, 1981, **39**, 341-3.
53 L.M. Malard, M. A. Pimenta, G. Dresselhaus and M. S. Dresselhaus, Physics Reports, 2009, **473**, 51-87.
54 P. Lespade, A. Marchand, M. Couzi and F. Cruege, *Carbon*, 1984, **22**, 375-85.